RSC Advances

PAPER

View Article Online
View Journal | View Issue

Cite this: *RSC Adv.*, 2022, **12**, 2383

Stearic acid modified nano CuMOFs used as a nitric oxide carrier for prolonged nitric oxide release†

Maotao Huang,[a] Jianwen Zhang,[a] Xianlan Ke,[a] Shuai Gao,[b] Dimeng Wu,[b] Junying Chen*[a] and Yajun Weng *[a]

Received 3rd November 2021
Accepted 9th January 2022

DOI: 10.1039/d1ra08066k

rsc.li/rsc-advances

Nitric oxide (NO) shows high potential in the cardiovascular system with anticoagulant and antibacterial efficacy. Cu based metal organic frameworks with amino modification (CuMOFs) were found to have an extraordinary high NO loading, but at the expense of framework stability in ambient moisture. Nano CuMOFs was synthesized by hydrothermal method in this work, and treated with stearic acid (SA) creating a hydrophobic form. It was found that the structure of the particles was not affected after treatment with SA, and the treated CuMOFs had tunable hydrophobicity. Both CuMOFs and SA modified CuMOFs adsorbed NO with the reaction of the amino group and NO to form a NONOate. SA modification enhanced stability of the CuMOFs in phosphate buffer solution (PBS, pH = 7.4), slowed down the interaction between the NO loading unit and H_2O, and thus NO releasing was prolonged. The resulting NO-loaded CuMOFs inhibited platelet activation dramatically, prolonged the coagulation time and displayed excellent antibacterial properties. They could be envisioned as a good candidate for application in blood contacting implants.

1. Introduction

Nitric oxide (NO) is a critical biological signaling molecule, which is endogenously produced and plays a central role with different functions such as antibacterial, antithrombotic, and wound healing.[1–3] A large body of evidence[2,4] shows that NO, in addition to regulating vascular tone, has important anti-vascular sclerotic effects, mainly in the form of anti-platelet effects, among others.[5] In addition, NO is a potent antibacterial and antiviral agent. NO induces nitrosation and oxidative stress to directly modify membrane proteins *via* reactive substances, which are thought to play a crucial role in antibacterial activity.[6,7] Such reactive substances may include NO radicals (NO), nitrogen dioxide (NO_2), nitrous oxide (N_2O_3), and peroxynitrite ($ONOO^-$).[8] In antimicrobial applications, NO is effective in killing not only single strains of bacteria but also mixed microbial strains. Therefore, NO is considered as a potential therapeutic agent for anti-thrombotic and anti-microbial applications.[9,10]

NO delivery technologies using solid storage materials are increasingly significant. Examples of NO carriers currently investigated mainly include NONOates,[11,12] metal exchanged zeolites,[13] and metal–organic frameworks (MOFs).[14] NONOates were among the first compounds to be studied for potential NO delivery, and are molecular species capable of releasing chemically bound NO upon contact with water. Alternatively, one of the most promising candidates for NO delivery is currently the use of porous materials, especially MOFs. MOFs represent a class of hybrid organic–inorganic porous materials that have attracted a lot of interest because of their chemical tunability, high porosities, and good thermal stability. They can be activated in vacuum at high temperature to obtain coordinatively unsaturated metal sites (CUSs) on the walls of the pores, which are available for binding of small molecules. Among the various MOFs, CuBTC (also known as HKUST-1) is one of the highly studied MOFs with CUSs, for which applications in NO delivery have been demonstrated.[15] Recently, the amino functionalized MOF, $Cu_3(NH_2BTC)_2$ (ref. 16) was used to load NO which showed NONOate formation additional to the coordination of NO to unsaturated copper centers.[17]

However, one of the major shortcomings of MOFs is their instability in the presence of moisture, and some researchers tried to enhance its stability in water or PBS. For example, a modified CuBTC with plasma enhanced chemical vapor deposition of perfluorohexane was reported by Decoste *et al.* to prevent the formation of water clusters around the Cu sites.[18] Rani *et al.* reported that HKUST-1 post-synthetically modified with amino acids showed transition behavior from hydrophilic to hydrophobic, and thus had better stability in aqueous environment.[19] Moreover, for enhancing hydrophobic small molecule capture, materials or solvents were tailored for

[a]*Key Laboratory of Advanced Technologies of Materials, Ministry of Education, School of Materials Science and Engineering, Southwest Jiaotong University, Chengdu, PR China. E-mail: chenjunying@swjtu.edu.cn; wengyj7032@swjtu.edu.cn*

[b]*Chengdu Daxan Innovative Medical Tech. Co., Ltd, Chengdu, PR China*

† Electronic supplementary information (ESI) available. See DOI: 10.1039/d1ra08066k

increased hydrophobicity.[20–22] To obtain a sustained NO release, Mondal *et al.* reported a highly hydrophobic polytetrafluoroethylene particle immobilization on NO releasing polymer to slow down interaction of NO releasing polymer with water molecules.[23]

In this study, Cu based MOFs was tailored with amino group and SA modification to obtain a super hydrophobic form and sustained NO release (Fig. 1). A hybrid linker coordinated CuMOFs was first prepared by hydrothermal method, which had amino group as a functional group to form NONOates when contacting NO. Then it was post-synthetically modified with stearic acid (SA) to obtain hydrophobic/superhydrophobic properties. Copper ion and NO release, and anticoagulant and antibacterial properties *in vitro* were evaluated.

2. Experimental

2.1 Materials

Copper(II) nitrate hydrate ($Cu(NO_3)_2 \cdot 3H_2O$), 1,3,5-benzenetricarboxylic acid (BTC, 98%), 2-aminoterephthalic acid (98%) and stearic acid (SA) were all purchased from Sigma Aldrich. Nitric oxide (99.9%) was purchased from Chengdu Shimao Gas Co. In addition, dialysis bag with a molecular weight cut-off MD44-300KD was used. Total Nitric Oxide Assay Kit (Beyotime Biotechnology, Shanghai, China) was used to detect NO release *in vitro*.

2.2 Preparation of CuMOFs and hydrophobic SA@CuMOFs

Nano CuMOFs was synthesized by a hydrothermal method. 1 g of BTC and 1 g of 2-aminoterephthalic acid were added into a solvent with 12 mL water and 30 mL anhydrous ethanol to form the mixed ligand solution. After ultrasonic treatment for 20 min, 20 mL $Cu(NO_3)_2$ solution with a concentration of 33 mM in water/ethanol (1 : 10) was added subsequently. Then it was ultrasonically treated for 20 min to obtain CuMOFs precursor solution. The precursor solution was kept in an autoclave for 1 h at 140 °C. After being taken out, the sample was centrifuged at 4000 rpm for 5 min, then washed two times with ethanol and dried at 80 °C for 5 h to get the final CuMOFs nanoparticles.

400 mg of CuMOFs was dispersed in ethanol solution, and SA was added to obtain a final concentration of 0 mg mL^{-1}, 0.625 mg mL^{-1}, 2.5 mg mL^{-1} and 10 mg mL^{-1} respectively. After being ultrasonically treated for 30 min, the samples were centrifuged at 12 000 rpm for 10 min and dried for 5 h at 80 °C. The obtained samples were referenced to as SA_1@CuMOFs, SA_2@CuMOFs, SA_3@CuMOFs which represented SA concentration of 0.625 mg mL^{-1}, 2.5 mg mL^{-1} and 10 mg mL^{-1} respectively.

2.3 NO loading and releasing

The CuMOFs and SA_3@CuMOFs were activated under vacuum at a temperature of 100 °C for 6 h for further NO loading. After being cooled down to room temperature, the samples were transferred to a NO filling device. The pressure of the device chamber was first evacuated with a vacuum pump for 30 minutes and then exposed to NO at 1 MP for 8 hours. The obtained samples were labeled as NO@CuMOFs and NO@SA_3@CuMOFs respectively.

NO release was measured using the total NO assay kit. NO can be easily transferred into nitrite and nitrate in water. For total NO assay, nitrate in the solution was reduced to nitrite by nitrate reductase and the total nitrite was quantitatively detected by classical Griess reagent. Details was as follows. First, 1 M $NaNO_2$ was diluted with PBS to 2, 5, 10, 20, 40, 60 and 80 μmol L^{-1} to get a standard curve. Second, 100 mg of NO@CuMOFs and NO@SA_3@CuMOFs was placed into the prepared dialysis tape respectively, and then incubated in 100 mL PBS at 37 °C. At each of the preset time, the solution was analyzed for NO release according to the total NO assay kit.

2.4 Characterization

The surface morphological features of samples were studied using the JSM-7800F field emission scanning electron microscope (SEM). The composition and crystal structure were characterized by using X-ray powder diffraction (XRD). The hydrophilic and hydrophobic properties were evaluated by

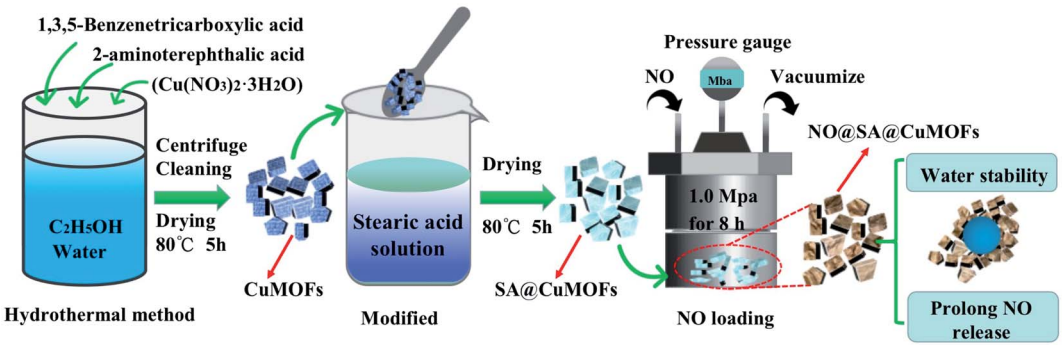

Fig. 1 Schematic illustration of the preparation of CuMOFs, SA@CuMOFs and NO@SA@CuMOFs.

using a JC2000 contact angle test system with 5 μL water droplet chosen as the test liquid. The information on functional groups and chemical bonds were detected after materials were well mixed and ground with KBr *via* FTIR. All the tests were performed at ambient temperature. All optical videos and photos were obtained by using a digital camera.

2.5 Anticoagulation and antibacterial biology of CuMOFs

Platelet-rich plasma (PRP) was obtained by centrifuging fresh anticoagulant rabbit blood at 1500 rpm for 15 minutes. 10 mg of CuMOFs and NO@SA_3@CuMOFs were added in a Millipore transwell chamber respectively, and placed in the wells of a 24-well cell culture plate. Then 1 mL of PRP was added to each well. After incubation at 37 °C for 60 min, the plates were washed three times with PBS (pH = 7.4) and then fixed with 2.5% glutaraldehyde overnight. After gradient dehydration, prepared samples were examined by SEM. Each sample was tested in triplicate.

For coagulation time test, 500 μL fresh whole blood without anticoagulant and 10 mg of CuMOFs or NO@SA3@CuMOFs were simultaneously added into a 24-well cell culture plate. After incubation for a preset time (20 min, 40 min and 60 min) at 37 °C, 2 mL of physiological saline was added. The coagulated clots will precipitate and 50 μL supernatant was transferred to a new plate. After 2 mL of physiological saline was added, absorbance at 545 nm was detected.

The antibacterial potency of CuMOFs, NO@CuMOFs and NO@SA_3@CuMOFs against *E. coli* and *S. epidermidis* was investigated by the minimal inhibitory concentration estimation and growth inhibition assay. The minimal inhibitory concentration of NO@SA_3@CuMOFs was evaluated as follows. The optical density (OD) of the cultures was adjusted to 0.2 at a wavelength of 600 nm (1.5×10^8 CFU mL^{-1}). Samples was first diluted with saline into series of concentration, and 10 mL of the series of diluted solution and 10 mL of agar medium was added into a Petri dish. After solidification, 2 μL of bacterial suspension was seeded and then incubated in a bacterial incubator at 37 °C for 24 hours. The minimal inhibitory concentration was determined by the highest dilution showing complete inhibition of the tested strain. For growth inhibition assay, the pre-cultured *E. coli* and *S. epidermidis* were diluted 100 times to obtain a test inoculum with a concentration of 1.5×10^6 CFU mL^{-1} 5 mL of the test inoculum was added into a tube, then 12.5 mg samples were added. After incubation at 37 °C for 24 hours, the surviving bacteria were collected into a new Petri dish by washing with 10 mL sterilized saline. Then 30 μL of 1.5×10^5 CFU mL^{-1} inoculum was seeded on agar to count the colonies after 24 h culture. The antibacterial rate was calculated according to the following formula

$$R = \frac{N_c - N_e}{N_c} \times 100\% \quad (1)$$

where R stands for antibacterial rate, N_c is the number of colonies on the blank and N_e is the number of colonies on the tested samples.

3. Results and discussions

3.1 Characterization of CuMOFs and SA@CuMOFs nanoparticles

The as-synthesized CuMOFs and SA@CuMOFs were characterized using SEM, FTIR, and XRD. As shown by SEM, the synthesized CuMOFs exhibited a laminar structure with an average size of 100–200 nm (Fig. 2a). In this work, mixed linkers of BTC and 2-aminoterephthalic acid (NH_2TPA) were used to prepare the amino group functionalized CuMOFs. CuBTC (HKUST-1) and Cu(NH_2TPA) was also prepared by using mono linker respectively under the same condition. The morphology of CuBTC is a three-dimensional octahedral structure, and that of Cu(NH_2TPA) is laminar structure similar with the as-synthesized CuMOFs (ESI Fig. S1†). 2-Aminoterephthalic acid is a linker similar with terephthalic acid (TPA). It was also mentioned that HKUST-1 is always coordinated in three dimensions, whereas CuTPA appears to have a lamellar geometry that forms two-dimensional tunnels.[24] The mix of NH_2TPA linker disturbed the space coordinates, thus resulted in a laminar structure. After SA post modification of the CuMOFs, it showed that the morphology did not change (Fig. 2a).

The CuMOFs and SA modified CuMOFs were dispersed in ethanol and a uniform coating was prepared on titanium foil by dipping and pulling for 5 times. Water contact angle was detected and it showed the surface with CuMOFs was superhydrophilic. The topography of the microstructure of the nanoparticle combined with surface charge of Cu(II) may both contributed to the super wettability. Whereas surfaces SA_1@CuMOFs, SA_2@CuMOFs, and SA_3@CuMOFs presented hydrophobic and superhydrophobic behavior with the contact angles of 62°, 109°, and 154° respectively (Fig. 2b). To reduce the interaction between water and the loaded NO cargo in the nanoparticles, SA_3@CuMOFs with superhydrophobic properties was chosen for the following studies.

FTIR spectra were recorded for the studied nanoparticles before and after SA modification. The distinct changes in FTIR spectra after SA modification are discussed below. The two characteristic peaks at 2919 and 2853 cm^{-1} assigned to C–H stretching of SA were apparently increased (Fig. 2c).[25] Vibration of functional group $-NH_2$ was overlapped with –OH of carboxylic group, which formed a wide absorption instead of a sharp peak around 3400–3500 cm^{-1} for both samples.

The crystallographic structure of the as-prepared samples is analyzed by powder X-ray diffraction (XRD). The X-ray diffraction (XRD) results showed significant diffraction peaks within 5–50° of 2θ and the position and relative intensity of the diffraction peaks of SA_3@CuMOFs and NO@SA@CuMOFs were mainly consistent with the typical HKUST-1 (ref. 26) (Fig. 2d). The CuMOFs has extremely intense diffraction peaks at 6.7°, 9.6°, 11.6° and 13.5°, which correspond to the (200), (220), (222), (400) lattice planes of HKUST-1 respectively. However, the other diffraction peaks of HKUST-1 at 16.6°, 19.1°, 24.3°, 26.1°, 29.5° and 35.5° are very weak, which correspond to the (422), (440), (220), (551), (731), (751), (951) planes, respectively.[27] There was rarely little change compared with the simulated HKUST-1,

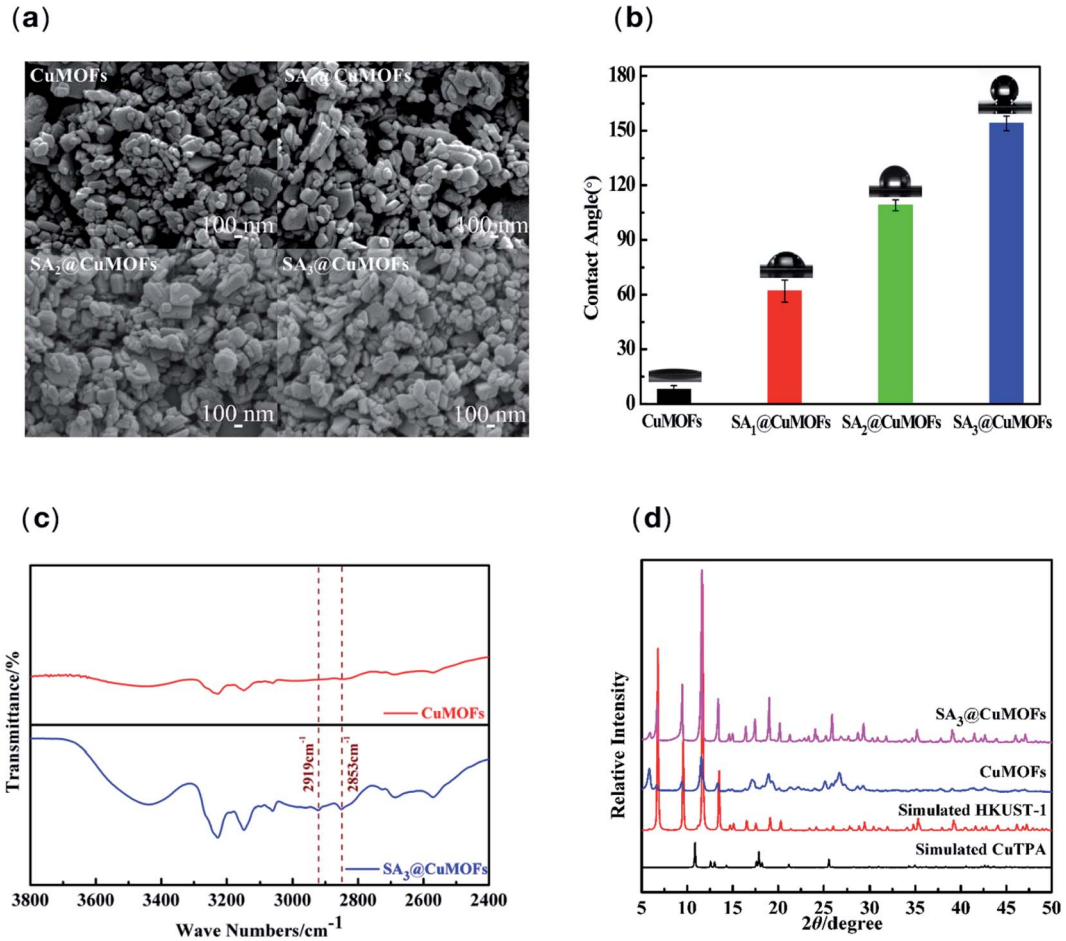

Fig. 2 Material characterization results of CuMOFs. (a) SEM images of CuMOFs, SA_1@CuMOFs, SA_2@CuMOFs, SA_3@CuMOFs, at 40 000× magnification; (b) contact angle measurements of CuMOFs, SA_3@CuMOFs; (c) FTIR spectra of CuMOFs, SA_3@CuMOFs, (d) XRD analysis of CuMOFs, SA_3@CuMOFs, with 2θ varied from 5 to 20°; the patterns were contrasted with the simulated HKUST-1 and CuTPA pattern.

indicating the CuMOFs and SA modified CuMOFs were HKUST-1 liked crystallographic structure.

3.2 NO loading and releasing

The FTIR spectra show only one significant difference for the NO-loaded MOFs compared to the unloaded MOFs: in the IR spectra of the NO-loaded MOFs samples a new peak at 1040 cm^{-1} is present (Fig. 3a and b). In addition, further changes of the NO-loaded status in their respective IR spectra can be revealed. It can be seen that the shoulder at 1292 cm^{-1} is slightly more pronounced in the NO-loaded MOFs which representing N=N stretching of the NONOate group.[28] Furthermore, a shift of absorbance at 940 cm^{-1} to 932 cm^{-1}, and the shoulder at 1683 cm^{-1} increased and sharped after NO loading. The signal around 1683 cm^{-1} is a characteristic of a –N=N–O group and therefore would indicate the formation of NONOate groups inside the MOFs.[16] The FTIR results indicated CuMOFs and SA_3@CuMOFs both can load NO *via* NONOate formation.

For sustained NO release, the stability of CuMOFs in PBS is critical. The CuMOFs and SA_3@CuMOFs were incubated in PBS for preset times, and Cu^{2+} ions concentration was measured. From the experimental results of Fig. 3c, the degradation rate of SA_3@CuMOFs in aqueous solution for the first 7 days was significantly decreased. The superhydrophobic property of SA_3@CuMOFs reduced the interaction between water and the MOFs to some extend, and delayed the degradation compared with that before SA modification.

NO release was shown in Fig. 3d. It can be seen that the bare CuMOFs particles loading with NO can release for about 72 h. After 72 h, the NO release of NO@CuMOFs is significantly slowed down and nearly not released. A total of 1.19 mmol of NO was released per gram of NO@CuMOFs. For NO@SA_3@-CuMOFs, although there was no significant difference for the first three days, however, it kept sustained NO release for 7 days. The cumulative release amount was 1.52 mmol per gram. It indicated SA may have the role of solubility enhancement of NO *via* hydrophobic interaction thus the loading amount increased.

The release time is one of concerned performances in the research of NO releasing materials. Many researches focused on improving the release time of NO. The comparison of the performance of NO releasing MOFs was showed in Table 1. It can be seen that NO@SA_3@CuMOFs investigated herein offer the highest released amount with a sustained NO release about

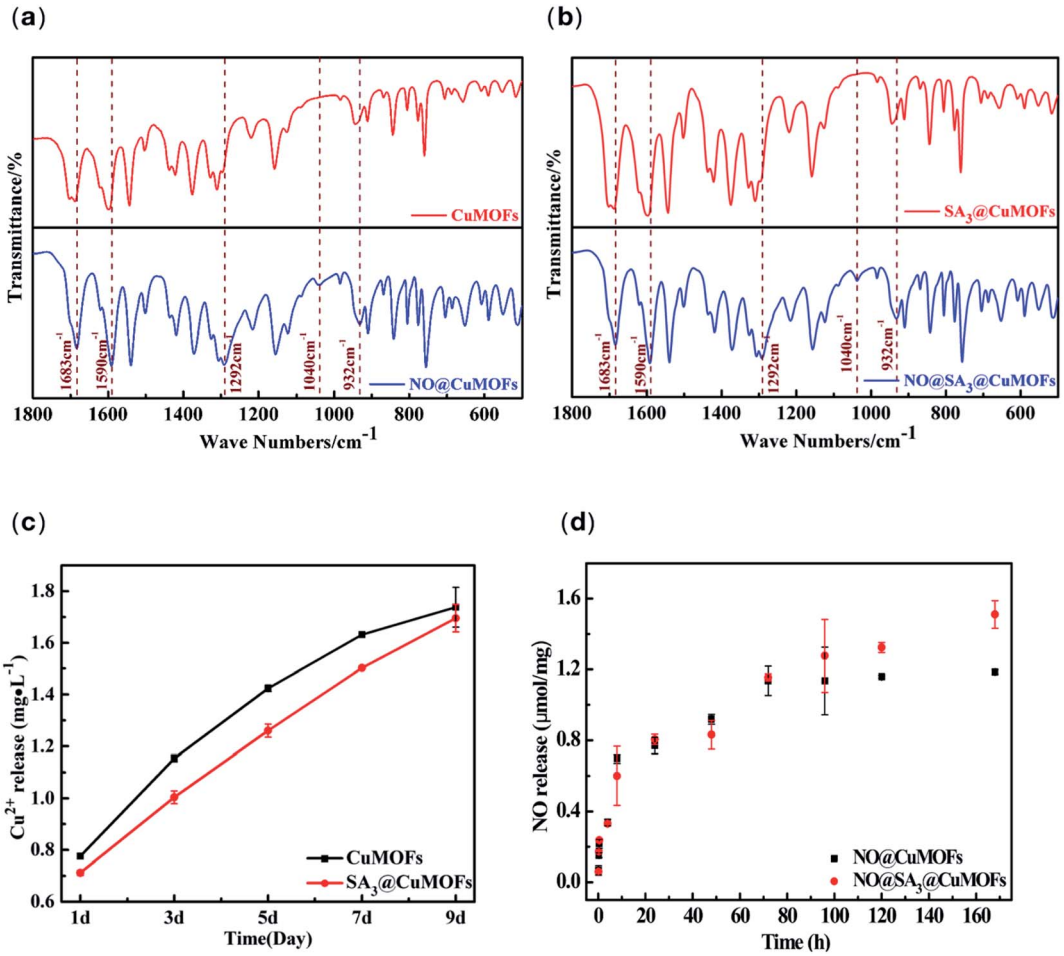

Fig. 3 Characterization of NO loading and releasing. (a) FTIR patterns of CuMOFs before and after loading NO; (b) FTIR patterns of SA_3@CuMOFs before and after loading NO; (c) cumulative release of copper ions from CuMOFs, SA_3@CuMOFs in PBS (pH = 7.4, 37 °C); (d) cumulative release of NO from CuMOFs, SA_3@CuMOFs in PBS (pH = 7.4, 37 °C) NO detected by the Griess assay. Values are expressed as mean ± standard deviation (SD) (n = 3).

168 h. The duration of NO release mainly depends on two factors. One is the stability of the frameworks, the other is the reaction rate of NO loading unit with H_2O. In the present study, SA modification not only enhanced the stability of the frameworks but also slowed down interaction of NO loading unit with water molecules. Both contributed to the long NO duration.

Table 1 Comparison of the performance of NO releasing MOFs

Material	Release conditions	Released amount	Duration of NO release	Ref.
CuMOFs	PBS	1.19 mmol g^{-1}	~72 h	This work
NO@SA_3@CuMOFs	PBS	1.52 mmol g^{-1}	~168 h	This work
UiO-66-NH_2	PBS/acid	1.1 mmol g^{-1}	~4 h	29
HKUST-1	11% relative humidity	0.001 mmol g^{-1}	Nearly complete after 20 min, continues for up to 60 min	30
Cu-TDPAT (diazeniumdiolated MOF)	85% relative humidity, room temperature	0.175 mmol g^{-1}	Initial burst in the first 3 h, then continued slower release in 168 h	31
NOF-11 (with bis-*N*-nitroso) moiety	Light irradiation	1.0 mmol g^{-1}	3600 s	32
MIL-100 (Fe)	11% relative humidity, 200 mL min^{-1}	0.55 mmol g^{-1}	Primarily released in first 2.5 h continues up to 25 h	33
UHM-37	11% relative humidity	0.0644 mmol g^{-1}	~6 h	34

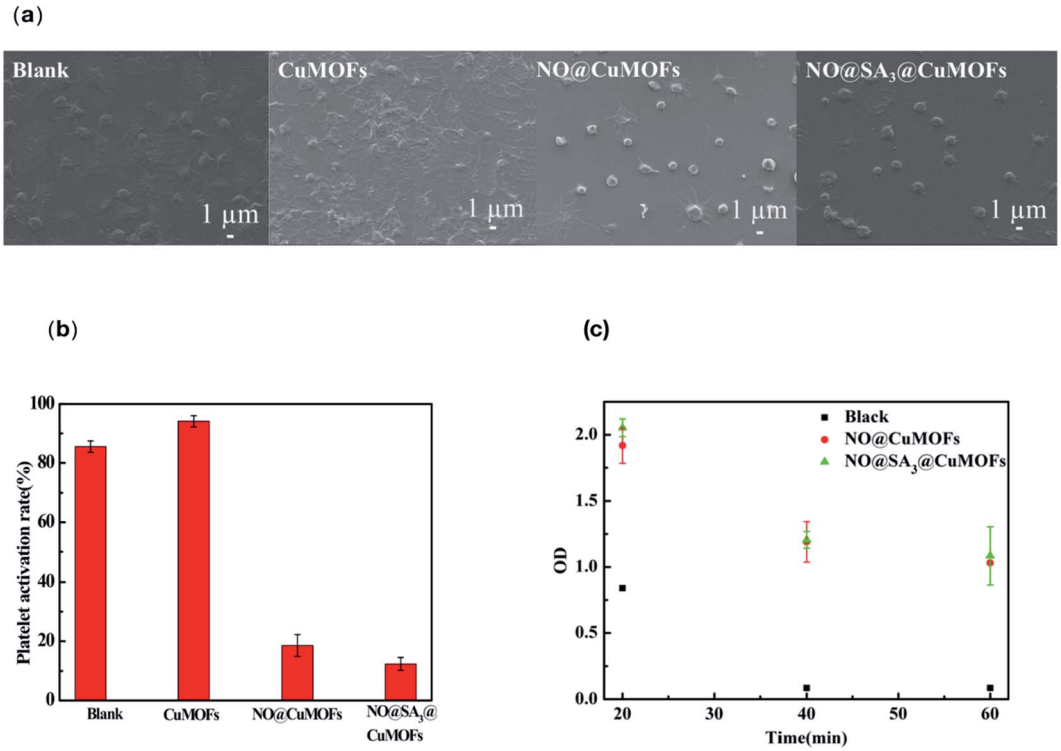

Fig. 4 *In vitro* anticoagulation evaluation of CuMOFs and SA_3@CuMOFs nanoparticles. (a) SEM images of platelet adhesion; (b) statistics analysis of platelet activation rate; (c) dynamic coagulation time of whole blood when contacting the samples.

3.3 Biological evaluation of the NO releasing CuMOFs

Up to now, the NO-releasing MOFs were mostly focused on NO loading and releasing, and few were about the biological function. Anticoagulant and antibacterial functions of the NO releasing MOFs of CuMOFs and SA_3@CuMOFs were evaluated in this research to explore the potential biological applications.

We tested the anticoagulation property of the as synthesized nanoparticles *in vitro*. Platelet adhesion on cell culture plate well was done, and samples were added in a Millipore transwell chamber which incubated within the PRP. As shown in Fig. 4a, the morphology of adhered platelets in both the blank and the CuMOFs groups displayed a spreading and fully spreading state, and the activation degree in the CuMOFs group was more pronounced. In contrast, most adhered platelets in the NO@CuMOFs and NO@SA_3@CuMOFs groups kept round or a little spreading state, which indicated that NO release from the samples and acting as an important platelet activation inhibitor. According to the statistics of activation rate, about 87% of the adhered platelet were activated in the blank group, while only 20% and 18% were activated with NO@CuMOFs and

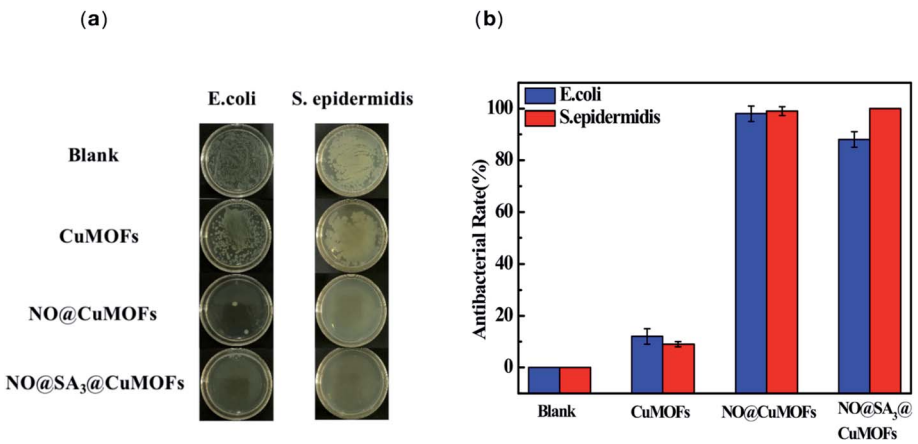

Fig. 5 Antimicrobial activity of CuMOFs particles and SA_3@CuMOFs. (a) Typical photographs of the bacterial colony of *E. coli* and *S. epidermidis* with samples incubation; (b) antibacterial rate of the samples against *E. coli* and *S. epidermidis*. Data are presented as the means ± SD ($n \geq 4$).

NO@SA_3@CuMOFs incubation respectively. But there is no significant difference in NO@CuMOFs and NO@SA_3@CuMOFs groups, this may be because that NO release in both groups for the first 1 h is approximately the same according to the experimental results in Fig. 4b.

Dynamic coagulation test is another indicator to evaluate the hemocompatibility of the material. After incubating the samples with fresh blood for 20, 40 and 60 minutes, 2 mL PBS was added and the supernatant was transferred to detect absorbance at 545 nm. When it was coagulated and precipitated, the supernatant changed transparent and the absorbance decreased. The results were showed in Fig. 4c, the absorbance of supernatant in both NO@CuMOFs and NO@SA_3@CuMOFs groups was significantly higher than that of the blank group, verifying that the NO loaded samples have an anticoagulant effect. Also, the anticoagulant capacity of NO@CuMOFs and NO@SA_3@CuMOFs is no significant difference.

The minimum inhibitory concentration of NO@SA_3@-CuMOFs sample against Gram-negative *E. coli* and Gram-positive *S. epidermidis* was detected (ESI Fig. S2†). It is both 2.5 mg mL^{-1} for *E. coli* and *S. epidermidis*. Fig. 5 shows the inhibitory effect of the different nanoparticles on *E. coli* and *S. epidermidis*. CuMOFs without SA modification showed a weak antibacterial efficacy at the concentration of 2.5 mg mL^{-1}. It can be seen that both NO loading groups had an significantly increased antibacterial function. The antibacterial rate of NO@SA_3@CuMOFs against *E. coli* was about 90%, and the antibacterial rate of NO@CuMOFs against *E. coli* was above 95%. While both reached almost 100% against *S. epidermidis*. The antibacterial rate of NO@CuMOFs against *E. coli* was slightly higher than that of NO@SA_3@CuMOFs, which may be because more initial Cu^{2+} release in this sample without SA modification.

Therefore, the results of this study indicate that the as synthesized NO-releasing CuMOFs have good anticoagulant and antibacterial activities, which are promising in application for blood contacting devices.

4. Conclusion

A hybrid linker with amino group was used to synthesize nano CuMOFs, and subsequent it was modified with SA for increased hydrophobicity. SA modification simultaneously enhanced stability of the CuMOFs in water and allowed for sustained NO releasing. FTIR results revealed that NONOates formation within NO loading in SA modified CuMOFs. NO releasing from the nanoparticles not only dramatically inhibited platelet activation *in vitro* but also significantly increased the antibacterial activity. It can be loaded in the coating of blood contact biomaterials in future to achieve excellent anticoagulant and antibacterial properties.

Conflicts of interest

There are no conflicts to declare.

Acknowledgements

This work was financially supported by the National Key Research and Development Program of China (No. 2020YFC1107303).

References

1 K. P. Reighard, C. Ehre, Z. L. Rushton, M. J. R. Ahonen, D. B. Hill and M. H. Schoenfisch, Role of Nitric Oxide-Releasing Chitosan Oligosaccharides on Mucus Viscoelasticity, *ACS Biomater. Sci. Eng.*, 2017, **3**, 1017–1026.
2 G. Reichanbach, S. Momi and P. Gresele, Nitric oxide and its antithrombotic action in the cardiovascular system, *Curr. Drug Targets: Cardiovasc. & Haematol. Disord.*, 2005, **5**, 65–74.
3 J. M. Malone-Povolny Malone, S. E. Maloney and M. H. Schoenfisch, Nitric Oxide Therapy for Diabetic Wound Healing, *Adv. Healthcare Mater.*, 2019, **8**, 1801210.
4 F. C. Munhoz, S. R. Potje, A. C. Pereira, M. G. Daruge and C. Antoniali, Hypotensive and vasorelaxing effects of the new NO-donor [Ru(terpy)(bdq)NO+](3+) in spontaneously hypertensive rats, *Nitric Oxide*, 2012, **26**, 111–117.
5 T. C. Major, D. O. Brant, C. P. Burney, K. A. Amoako, G. M. Annich, M. E. Meyerhoff, H. Handa and R. H. Bartlett, The hemocompatibility of a nitric oxide generating polymer that catalyzes S-nitrosothiol decomposition in an extracorporeal circulation model, *Biomaterials*, 2011, **32**, 5957–5969.
6 D. O. Schairer, J. S. Chouake, J. D. Nosanchuk and A. J. Friedman, The Potential of Nitric Oxide Releasing Therapies as Antimicrobial Agents, *Virulence*, 2012, **3**, 271–279.
7 H. Nurhasni, J. Cao, M. Choi, I. Kim, B. L. Lee, Y. Jung and J. W. Yoo, Nitric Oxide-Releasing Poly(Lactic-*co*-Glycolic Acid)-Polyethylenimine Nanoparticles for Prolonged Nitric Oxide Release, Antibacterial Efficacy, and *in vivo* Wound Healing Activity, *Int. J. Nanomed.*, 2015, **10**, 3065–3080.
8 M. L. Jones, J. G. Ganopolsky, A. Labbé, C. Wahl and S. Prakash, Antimicrobial properties of nitric oxide and itsapplication in antimicrobial formulations and medical devices, *Appl. Microbiol. Biotechnol.*, 2010, **88**, 401–407.
9 N. Naghavi, A. De Mel, S. O. Alavijeh, G. B. Cousins and M. A. Seifalian, Nitric oxide donors for cardiovascular implant applications, *Small*, 2013, **9**, 22–35.
10 J. Durão, N. Vale, S. Gomes, P. Gomes, C. C. Barrias and L. Gales, Nitric Oxide Release from Antimicrobial Peptide Hydrogels for Wound Healing, *Biomolecules*, 2018, **9**(1), 4.
11 T. Liu, G. Li, X. Wu, S. Chen, S. Zhang, H. Han, H. Zhang, X. Luo, X. Cai and D. Ma, B-Cyclodextrin-*graft*-poly(amidoamine) dendrons as the nitric oxide deliver system for the chronic rhinosinusitis therapy, *Drug Delivery*, 2021, **28**(1), 306–318.
12 J. L. Harding and M. M. Reynolds, Metal organic frameworks as nitric oxide catalysts, *J. Am. Chem. Soc.*, 2012, **134**, 3330–3333.
13 M. M. Reynolds, J. A. Hrabie, B. K. Oh, J. K. Politis, M. L. Citro, L. K. Keefer and M. E. Meyerhoff, Nitric oxide

releasing polyurethanes with covalently linked diazeniumdiolated secondary amines, *Biomacromolecules*, 2006, **7**, 987–994.

14 H. Zhang, G. M. Annich, J. Miskulin, K. Stankiewicz, K. Osterholzer, S. I. Merz, R. H. Bartlett and M. E. Meyerhoff, Nitric Oxide-Releasing Fumed Silica Particles: Synthesis, Characterization, and Biomedical Application, *J. Am. Chem. Soc.*, 2003, **125**, 5015–5024.

15 B. Xiao, P. S. Wheatley, X. B. Zhao, A. J. Fletcher, S. Fox, A. G. Rossi, I. L. Megson, S. Bordiga, L. Regli, K. M. Thomas and R. E. Morris, High-capacity hydrogen and nitric oxide adsorption and storage in a metal–organic framework, *J. Am. Chem. Soc.*, 2007, **129**, 1203.

16 K. Peikert, L. J. McCormick, D. Cattaneo, M. J. Duncan, F. Hoffmann, A. H. Khan, M. Bertmer, R. E. Morris and M. Froba, Tuning the nitric oxide release behavior of amino functionalized HKUST-1, *Microporous Mesoporous Mater.*, 2015, **216**, 118–126.

17 A. H. Khan, K. Peikert, F. Hoffmann, F. Michael and M. Bertmer, Nitric Oxide Adsorption in Cu3btc2-Type MOFs-Physisorption and Chemisorption as NONOates, *J. Phys. Chem. C*, 2019, **123**, 4299–4307.

18 J. B. Decoste, G. W. Peterson, M. W. Smith, C. A. Stone and C. R. Willis, Enhanced Stability of Cu-BTC MOF via Perfluorohexane Plasma-Enhanced Chemical Vapor Deposition, *J. Am. Chem. Soc.*, 2012, **134**, 1486–1489.

19 R. Reetu, D. Akash, M. Boris and S. Suman, Enhanced hydrothermal stability of Cu MOF by post synthetic modification with amino acids, *Vacuum*, 2019, **164**, 449–457.

20 P. M. Bhatt, B. Youssef, C. Amandine, A. Karim, S. Osama, S. Aleksander, L. J. Barbour and E. Mohamed, A Fine-Tuned Fluorinated MOF Addresses the Needs for Trace CO2 Removal and Air Capture Using Physisorption, *J. Am. Chem. Soc.*, 2016, **138**, 9301–9307.

21 P. D. Mobley, A. V. Rayer, J. Tanthana, T. R. Gohndrone and M. Lail, CO2 Capture Using Fluorinated Hydrophobic Solvents, *Ind. Eng. Chem. Res.*, 2017, **56**, 11958–11966.

22 X. N. Wu, B. Zhao, L. Wang, Z. H. Zhang, H. W. Zhang, X. H. Zhao and X. F. Guo, Hydrophobic PVDF/graphene hybrid membrane for CO2 absorption in membrane contactor, *J. Membr. Sci.*, 2016, **520**, 120–129.

23 A. Mondal, R. Devine, L. Estes, J. Manuel and H. Handa, Highly hydrophobic polytetrafluoroethylene particle immobilization via polydopamine anchor layer on nitric oxide releasing polymer for biomedical applications, *J. Colloid Interface Sci.*, 2021, **585**, 716–728.

24 C. Carson, K. Hardcastle, J. Schwartz, X. T. Liu, C. Hoffmann, G. A. Rosario and R. Tannenbaum, Synthesis and Structure Characterization of Copper Terephthalate Metal–Organic Frameworks, *Eur. J. Inorg. Chem.*, 2009, **16**, 2338–2343.

25 J. Li, H. Wan, Y. Ye, H. Zhou and J. Chen, One-step process for the fabrication of superhydrophobic surfaces with easy repairability, *Appl. Surf. Sci.*, 2012, **258**, 3115–3118.

26 E. Laurila, J. Thunberg, S. Argent, N. Champness, S. Zacharias, G. Westman and L. Ohrstrom, Enhanced Synthesis of Metal–Organic Frameworks on the Surface of Electrospun Cellulose Nanofibers, *Adv. Eng. Mater.*, 2015, **17**, 1282–1286.

27 S. S.-Y. Chui, S. M.-F. Lo, J. P. H. Charmant, A. G. Orpen and I. D. Williams, A Chemically Functionalizable Nanoporous Material [Cu3(TMA)2(H2O)3]n, *Science*, 1999, **283**, 1148–1150.

28 G. W. Li, S. Yu, W. Xue, D. Ma and W. Zhang, Chitosan-graft-PAMAM loading nitric oxide for efficient antibacterial application, *Chem. Eng. J.*, 2018, **347**, 923–931.

29 R. R. Haikal, C. Hua, J. J. Perry, D. O'Nolan, I. Syed, A. Kumar, A. H. Chester, M. J. Zaworotko, M. H. Yacoub and M. H. Alkordi, Controlling the Uptake and Regulating the Release of Nitric Oxide in Microporous Solids, *ACS Appl. Mater. Interfaces*, 2017, **9**, 43520–43528.

30 B. Xiao, P. S. Wheatley, X. Zhao, A. J. Fletcher, S. Fox, A. G. Rossi, I. L. Megson, S. Bordiga, L. Regli, K. M. Thomas and R. E. Morris, High-capacity hydrogen and nitric oxide adsorption and storage in a metal–organic framework, *J. Am. Chem. Soc.*, 2007, **129**, 1203–1209.

31 A. Lowe, P. Chittajallu, Q. Gong, J. Li and K. J. Balkus, Storage and delivery of nitric oxide via diazeniumdiolated metal organic framework, *Microporous Mesoporous Mater.*, 2013, **181**, 17–22.

32 C. Kim, S. Diring, S. Furukawa and S. Kitagawa, Light–induced nitric oxide release from physiologically stable porous coordination polymers, *Dalton Trans.*, 2015, **44**, 15324–15333.

33 J. F. Eubank, P. S. Wheatley, G. Lebars, A. C. McKinlay, H. Leclerc, P. Horcajada, M. Daturi, A. Vimont, R. E. Morris and C. Serre, Porous, rigid metal(III)-carboxylate metal–organic frameworks for the delivery of nitric oxide, *APL Mater.*, 2014, **2**, 124112.

34 J. Gascon, U. Aktay, M. Hernandez-Alonso, G. P. M. van klink and F. Kapteijn, Amino-based metal–organic frameworks as stable, highly active basic catalysts, *J. Catal.*, 2009, **261**, 75–87.